ELSEVIER

Biochimica et Biophysica Acta 1417 (1999) 51–62

BIOCHIMICA ET BIOPHYSICA ACTA
BBA

# Membrane dielectric responses of human T-lymphocytes following mitogenic stimulation

Ying Huang *, Xiao-Bo Wang, Peter R.C. Gascoyne, Frederick F. Becker

*Department of Molecular Pathology, The University of Texas M.D. Anderson Cancer Center, 1515 Holcombe Boulevard, Houston, TX 77030 USA*

Received 8 October 1998; received in revised form 10 December 1998; accepted 10 December 1998

**Abstract**

Human peripheral blood T-lymphocytes, normally resting at the $G_0$ phase, were stimulated with phytohemagglutinin (PHA) and interleukin-2 (IL-2) to induce the cell division cycle. The cells were examined at 24-h intervals for up to 96 h by flow cytometry to determine cell cycle distributions and by electrorotation to determine dielectric properties. The average membrane specific capacitance was found to vary from 12 ($\pm$1.5) mF/m$^2$ prior to stimulation to 10 ($\pm$1.5) and 16 ($\pm$3.5) mF/m$^2$ at 24 and 48 h after stimulation, respectively, and to remain unchanged up to 96 h after stimulation. Scanning electron microscopy studies of the cells revealed an increased complexity in cell membrane morphology following stimulation, suggesting that the observed change in the membrane capacitance was dominated by the alteration of cell surface structures. The average electrical conductivity of the cell interior decreased from $\sim$1.1 S/m prior to stimulation to $\sim$0.8 S/m at 24 h after stimulation and showed little change thereafter. The average dielectric permittivity of the cell interior remained almost unchanged throughout the course of the cell stimulation. The percentage of T-lymphocytes in the S and $G_2$/M phases increased from $\sim$4% prior to stimulation to $\sim$11 and $\sim$34% at 24 and 48 h after stimulation, respectively. The large change in membrane specific capacitance between the 24 and 48 h time period coincided with the large alteration in the cell cycle distribution where the S and $G_2$/M populations increased by $\sim$23%. These data, together with an analysis of the variation of the membrane capacitance during the cell cycle based on the cell cycle-dependent membrane lipid accumulation, show that there is a correlation between membrane capacitance and cell cycle phases that reflects alterations in the cell plasma membrane. © 1999 Elsevier Science B.V. All rights reserved.

*Keywords:* Electrorotation; Membrane capacitance; Cell dielectric phenotype; T-cell stimulation; Cell cycle; Cell surface morphology

## 1. Introduction

Electrorotation (ROT), the spinning of cells in a rotating electric field, has been widely employed as a method to characterize dielectric properties of individual cells [1–13]. We and others have reported ROT investigations of many cell types, such as rabbit oocytes [2], murine lymphocytes [3], yeast [4,5], human erythrocytes [11–13], and a number of cancer cell lines [6–8,10,14,15]. These studies have revealed that cells of different types and cells in different physiological states possess unique, effective dielectric properties that are determined by cell structures and compositions. This finding has led to the concept of a cell dielectric phenotype, the relationship between the frequency dependency of the cell electro-

* Corresponding author. Fax: +1 (713) 792-5940; E-mail: ying@solace.mdacc.tmc.edu

0005-2736/99/$ – see front matter © 1999 Elsevier Science B.V. All rights reserved.
PII: S0005-2736(98)00253-3

kinetic properties and cellular structure and function. Novel dielectrophoresis based methods of cell manipulation and separation are being developed to exploit the differences in the dielectric phenotypes between different cell types [14–17].

Dielectric characterization of lymphocytes has been undertaken by several groups [3,18–20]. Using dielectric impedance measurement of cell suspension, Surowiec et al. [19] and Asami et al. [20] derived dielectric parameters of mouse and human peripheral blood lymphocytes, respectively. For example, a membrane specific capacitance of 8.6 mF/m$^2$ was determined for mouse lymphocytes. Ziervogel et al. [18] applied ROT to study human T-lymphocytes and demonstrated qualitatively that ROT spectra allowed the discrimination between unstimulated and stimulated human lymphocytes. A study of electrical properties of mouse T- and B-lymphocytes after the mitogenic stimulation was conducted by Arnold and his co-workers [3] using the ROT method. The membrane specific capacitance was found to increase from 7.6 mF/m$^2$ prior to stimulation to 13.5 mF/m$^2$ at 72 h after stimulation. To increase our understanding of the biological factors that influence the cell dielectric properties, we measured the ROT spectra and cell cycle distribution of human peripheral blood T-lymphocytes following their mitogenic stimulation and investigated the possible correlation between cell dielectric properties and phases in the cell division cycle.

## 2. Materials and methods

### 2.1. T-lymphocyte preparation and stimulation

Human T-lymphocytes were isolated from buffy bags (Gulf Coast Blood Bank, Houston, TX) as described previously [21,22]. Briefly, mononuclear cells were separated from buffy bags by density gradient centrifugation through Histopaque 1077 medium (Sigma Chemical, St. Louis, MO) in which the mononuclear cells were harvested after centrifugation from the interface between plasma and the medium. T-lymphocytes were then collected by rosetting mononuclear cells with neuraminidase- (Calbiochem, La Jolla, CA) treated sheep erythrocytes for 20 h, followed by centrifugation through the Histopaque medium. The pelleted cells were subsequently treated with lysing solution consisting of 8.26 g/l $NH_4Cl$, 1.0 g/l $KHCO_3$, and 0.037 g/l EDTA tetra sodium (Sigma) for 5 min at 4°C to lyse the sheep erythrocytes. Purified T-lymphocytes were then recovered in RPMI 1640 medium containing 10% fetal bovine serum (FBS), 1 mM glutamine, 20 mM HEPES buffer, and penicillin–streptomycin antibiotics for 3 h. In order to stimulate the T-lymphocytes to proliferate in vitro, 0.5% rehydrated phytohemagglutinin (PHA) (Gibco BRL, Gaithersburg, MD) and 1.70 ng/ml (17.0 U/ml) human recombinant interleukin-2 (IL-2) (Gibco BRL) in RPMI 1640 medium were used [23]. Cells were harvested at 24-h intervals up to 96 h for study either by flow cytometry to determine the cell cycle kinetics or by ROT to determine their dielectric properties.

### 2.2. Immunophenotyping

Immunophenotyping of the purified T-lymphocyte population was performed on a FACS analyzer (Becton Dickinson, San Jose, CA) on the basis of the T-cell associated marker CD3, B-cell antigen CD20, and monocyte-related antigen CD14. Aliquots of $10^6$ cells suspended in 100 μl RPMI 1640 containing 2% FBS were incubated in the dark on ice for 45 min in the presence of 10 μl of FITC-conjugated CD antibodies (Dako, Carpinteria, CA) or $IgG_1$ or $IgG_{2a}$ negative controls (Dako). Cells were then washed and resuspended at a concentration of $10^6$/ml in RPMI 1640. The green fluorescence (510–550 nm) of FITC was then detected with the FACS analyzer using excitation at $490 \pm 10$ nm from a doped mercury-arc lamp. Percentages of $CD3^+$, $CD20^+$, and $CD14^+$ cells were determined.

### 2.3. Cell cycle analysis

Propidium iodide (PI) (Sigma) was used to quantify cellular DNA contents and to determine the distribution of cells in $G_0/G_1$, S, and $G_2$/M phases. $10^6$ cells in 100 μl phosphate-buffered saline (PBS) were fixed on ice in 1 ml 70% ethanol for 1 h. The cells were harvested, resuspended at a concentration of $10^6$/ml in RPMI 1640, and then incubated at 37°C for 30 min in the presence of 40 μg/ml PI and 100 μg/ml RNase A (Boehringer Mannheim, Indianapolis,

IN). Finally, cells were analyzed on the FACS analyzer for Coulter volume and DNA content. Histograms of DNA content revealed that the cell phase distribution and contour plots of DNA content versus Coulter volume indicated the relationship between the cell growth phase and size.

### 2.4. Scanning electron microscopy (SEM)

Resting and stimulated T-lymphocytes were washed once with RPMI 1640 medium without serum, and the harvested cells were resuspended in isotonic sucrose solution (8.75% w/w) for 15 min so that cells examined by SEM would be in a similar state to those in ROT measurements. The cells were then fixed in modified Karnovsky's fixative (pH 7.5, adjusted to an osmolality of 295 mosmol/kg with sucrose solution) at 37°C for at least 30 min. The cells were then washed in 100 mM sodium cacodylate buffer (pH 7.3, adjusted with HCl) and stored in the same buffer in the refrigerator overnight. The cells were then post-fixed, rinsed, prepared, and examined on a Hitachi Model S520 scanning electron microscope as described previously [7,10].

### 2.5. Electrorotation measurements and data analysis

Our routine ROT procedure was used for cell dielectric characterization [7,8,10,14,15]. Briefly, cells suspended at a concentration of $5\times10^4$/ml in isotonic 8.5% (w/w) sucrose plus 0.3% (w/w) dextrose buffer adjusted to a conductivity of 56 mS/m with RPMI medium were allowed to sediment onto the glass substrate of a 400-μm polynomial electrode [4,24]. A rotating electric field between 1 kHz and 100 MHz was established by applying four sinusoidal signals (0.92 V RMS) in phase quadrature to the four poles of the electrode array. Rotation rates of individual cells located between the electrode tips were timed at four points per decade of frequency using a stopwatch.

ROT spectra were measured for about 10 T-lymphocytes at 24-h intervals for up to 96 h after stimulation, and the spectra were then analyzed to derive cell dielectric parameters. For the cells at 48, 72, and 96 h after stimulation, a wide spread in cell size distribution was observed. A deliberate choice of the larger cells for the ROT measurement was made so that we could measure cells that had responded to mitogenic stimulation and were in the S and $G_2$/M phases of the cell cycle. To verify the reproducibility of the results, three sets of T-lymphocyte stimulation experiments were conducted.

It is well established that the cell rotation rate depends on the imaginary part of the polarization factor, $\mathrm{Im}(f_{CM})$, and is given by (e.g. [1,7,10]),

$$R_{ROT} = -\frac{\varepsilon_m k^2 V^2}{2\eta}\mathrm{Im}(f_{CM}) \quad (1)$$

In this equation, $\eta$ is the medium dynamic viscosity, $k$ is a constant relating to the electrode geometry and the cell position inside the electrode chamber, $V$ is the applied voltage, and $\varepsilon_m$ is the dielectric permittivity of the suspending medium. The polarization factor (Clausius-Mosotti) $f_{CM} = (\varepsilon^*_{ceff}-\varepsilon^*_m)/(\varepsilon^*_{ceff}+2\varepsilon^*_m)$ depends on the complex permittivities of the cell and its suspending medium. In this work, the single-shell dielectric model [1,4,7], in which a cell is considered to be a conducting sphere (cell interior) surrounded by a poorly conducting shell (cell membrane), was used to characterize the cell dielectric properties. In this case, the effective complex permittivity $\varepsilon^*_{ceff}$ of a cell is given by

$$\varepsilon^*_{ceff} = \varepsilon^*_{mem}\frac{\left(\frac{r}{r-d}\right)^3 + 2\left(\frac{\varepsilon^*_{int}-\varepsilon^*_{mem}}{\varepsilon^*_{int}+2\varepsilon^*_{mem}}\right)}{\left(\frac{r}{r-d}\right)^3 - \left(\frac{\varepsilon^*_{int}-\varepsilon^*_{mem}}{\varepsilon^*_{int}+2\varepsilon^*_{mem}}\right)} \quad (2)$$

where $r$ is the cell radius; $d$ is the membrane thickness (= 4.5 nm) and $\varepsilon^*_{mem}$ and $\varepsilon^*_{int}$ are complex permittivities of plasma membrane and cytoplasm, respectively. In each $\varepsilon^* = \varepsilon - j\sigma/\omega$, $\omega$ is the angular frequency, $\sigma$ and $\varepsilon$ are the electrical conductivity and permittivity, respectively. In this single shell model, the four dielectric parameters used to characterize cells are the membrane specific capacitance ($C_{mem} = \varepsilon_{mem}/d$) and conductance ($G_{mem} = \sigma_{mem}/d$) and the cell interior conductivity ($\sigma_{int}$) and permittivity ($\varepsilon_{int}$). An optimization algorithm was used to determine the best fit of Eqs. 1 and 2 to experimental data and thereby to provide estimates for the parameters of $C_{mem}$, $\sigma_{int}$, $\varepsilon_{int}$. The effect of the membrane conductance ($G_{mem}$) on ROT spectra was made negligibly small by choosing a moderately high suspension-conductivity of 56 mS/m for ROT measurement

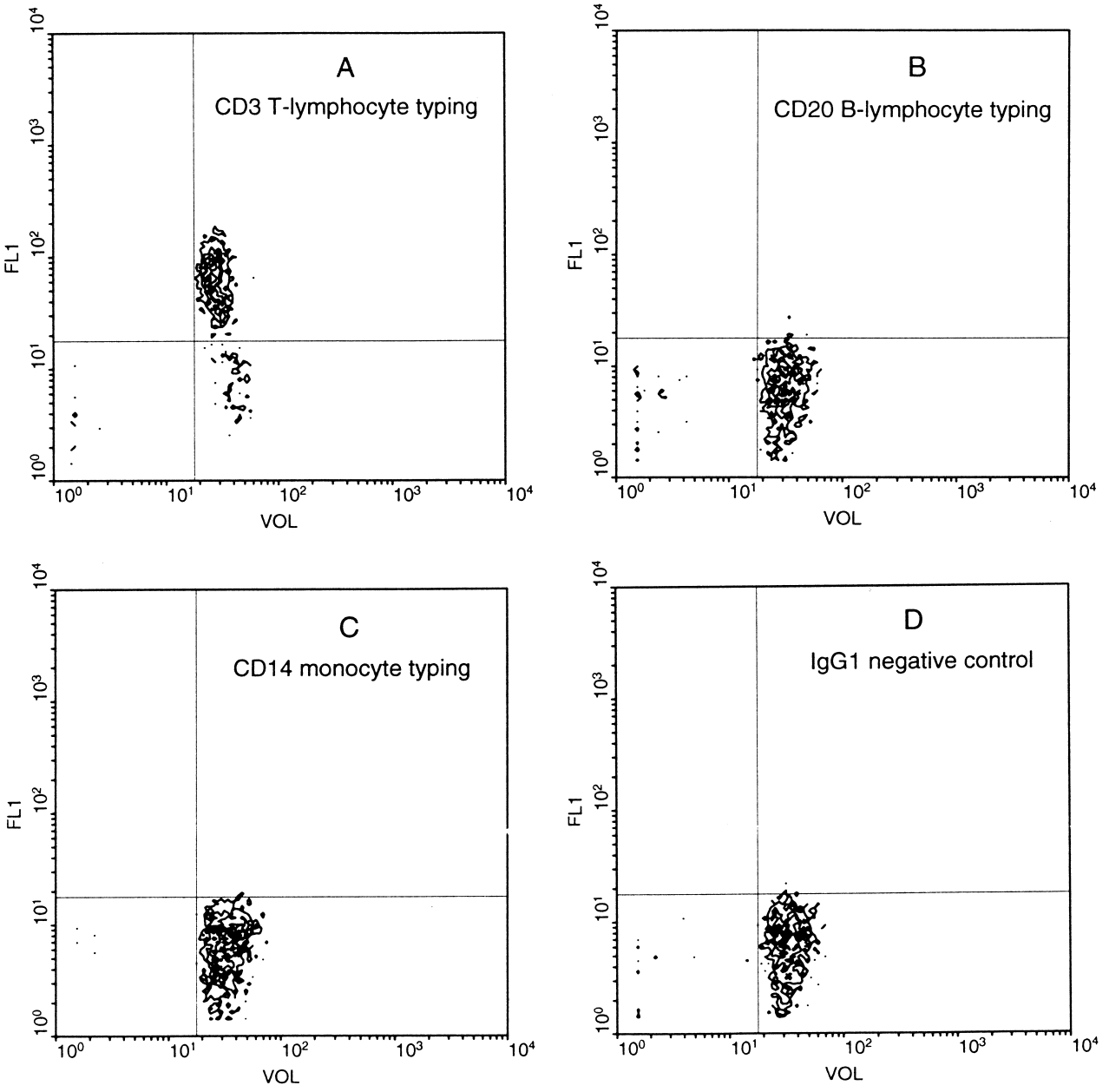


Fig. 1. Contour plot of FITC fluorescence vs. volume for: (A) T-, (B) B-lymphocyte and (C) monocyte typing with CD3, CD20, and CD14 markers, respectively, and (D) $IgG_1$ negative control of CD3 and CD20 typing. Over 95% of the cells exhibited $CD3^+$, whereas $< 5\%$ exhibited $CD20^+$ or $CD14^+$, indicating that the majority of the cell population is T-lymphocytes.

so that variations in $G_{mem}$ among different cells would have little influence on measured ROT responses [25]. As typical $G_{mem}$ values for viable mammalian cells were found to lie between 20 and 200 S/m$^2$ (including the case for activated murine T-lymphocytes [3]), $G_{mem}$ was fixed at 100 S/m$^2$ for the optimization.

## 3. Results

### 3.1. Immunophenotyping

In order to determine the percentage of T-, and B-lymphocytes, and monocytes in the purified T-cell population, immunotyping based on cell surface anti-

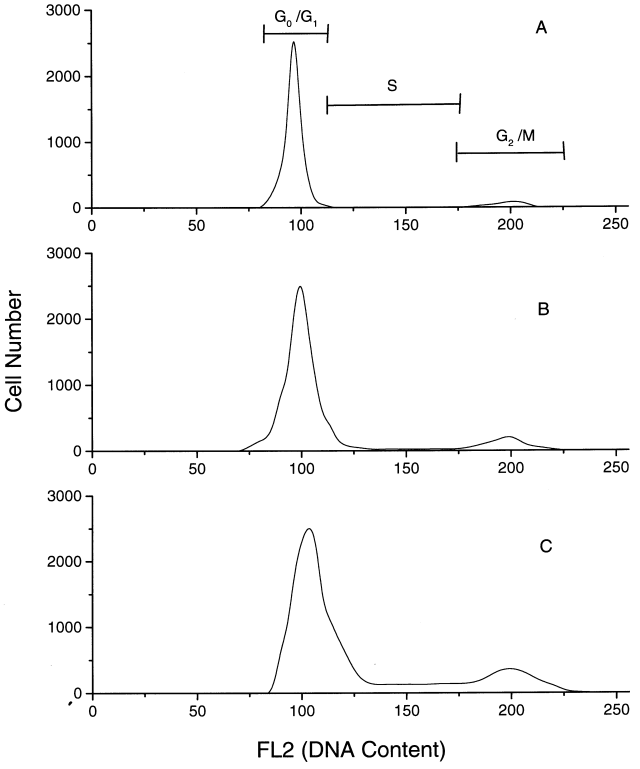


Fig. 2. DNA histogram of T-lymphocytes at: (A) 0, (B) 24, and (C) 48 h after mitogenic stimulation as determined from the FACS analyzer.

gens was performed using a FACS analyzer. Fig. 1A–C shows contour plots of FITC fluorescence vs. volume for typing T-, B-lymphocytes and monocytes with FITC-labeled CD3, CD20, and CD14 antibodies, respectively. Over 95% of the cells presented positive for the T-cell antigen CD3 with $<5\%$ of the cells being $CD20^+$ or $CD14^+$. The $IgG_1$ negative control of CD3 and CD20 typing, shown in Fig. 1D demonstrates that $<3\%$ of the cells exhibited $IgG_1{}^+$, indicating that little non-specific binding occurred.

### 3.2. Cell cycle analysis

Following the mitogenic stimulation, the cell cycle distribution of T-lymphocytes was determined by measuring cell DNA contents with the FACS analyzer. Fig. 2 shows typical PI fluorescence histograms for T-lymphocytes harvested at 0, 24, and 48 h after stimulation, illustrating that the S and $G_2$/M populations increased with time. The time dependency of the cell cycle distribution is summarized in Table 1. As expected, the percentage of cells in $G_0/G_1$ phase decreased with time after stimulation as more cells entered S and $G_2$/M phases of the division cycle. For example, prior to stimulation, $\sim$95% of the cells were in $G_0/G_1$ phase. At 48 h after stimulation and thereafter, more than one-third of the cells were in S and $G_2$/M phases, leaving $\sim$65% of the cells in $G_0/G_1$. The largest changes in cell cycle distribution occurred between 24 and 48 h after cell activation when S and $G_2$/M populations increased from $\sim$11 to $\sim$34%. Only a small change ($<2\%$ for each phase) was observed for the cell cycle distribution at 48–96 h after stimulation.

Another indicator that cells had left the $G_0$ resting state and had entered the cell division cycle was the observation that the mean Coulter volume of the cells increased by more than 150% at 48 h after stimulation (data not shown).

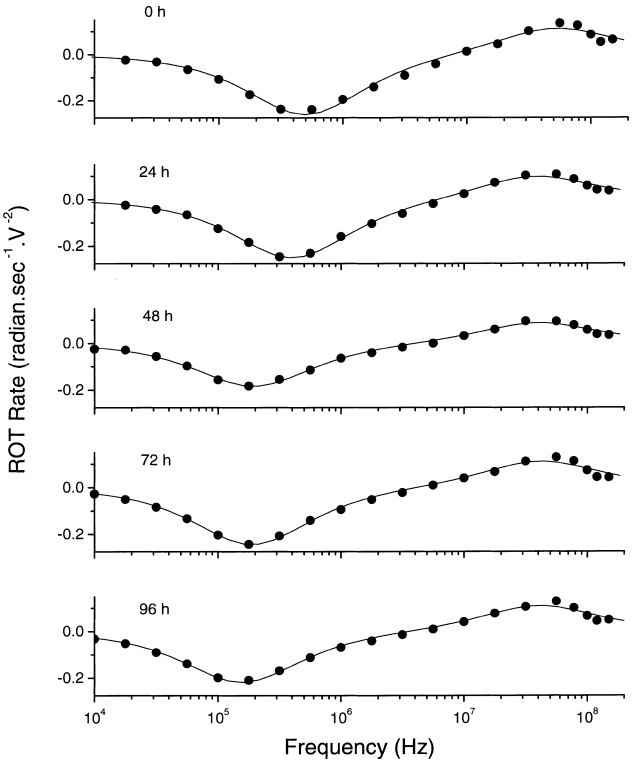


Fig. 3. Typical ROT spectra of T-lymphocytes at 0, 24, 48, 72, and 96 h after mitogenic stimulation. The cells were suspended in an isotonic sucrose/dextrose medium having an electric conductivity of 56 mS/m.

### 3.3. Electrorotation spectra

Typical ROT spectra for T-lymphocytes after the PHA/IL-2-induced mitogenic stimulation are shown in Fig. 3. The general features of ROT spectra of biological cells have been described previously [1]. Here, for T-lymphocytes, the antifield peak of ROT spectra shifted towards lower frequencies following the cell stimulation. For example, while the antifield peak rotation for a cell prior to stimulation occurred at ~500 kHz, by 96 h after stimulation the peak frequency fell to ~100 kHz for a cell. There was no significant change in the cofield ROT peak frequency after stimulation.

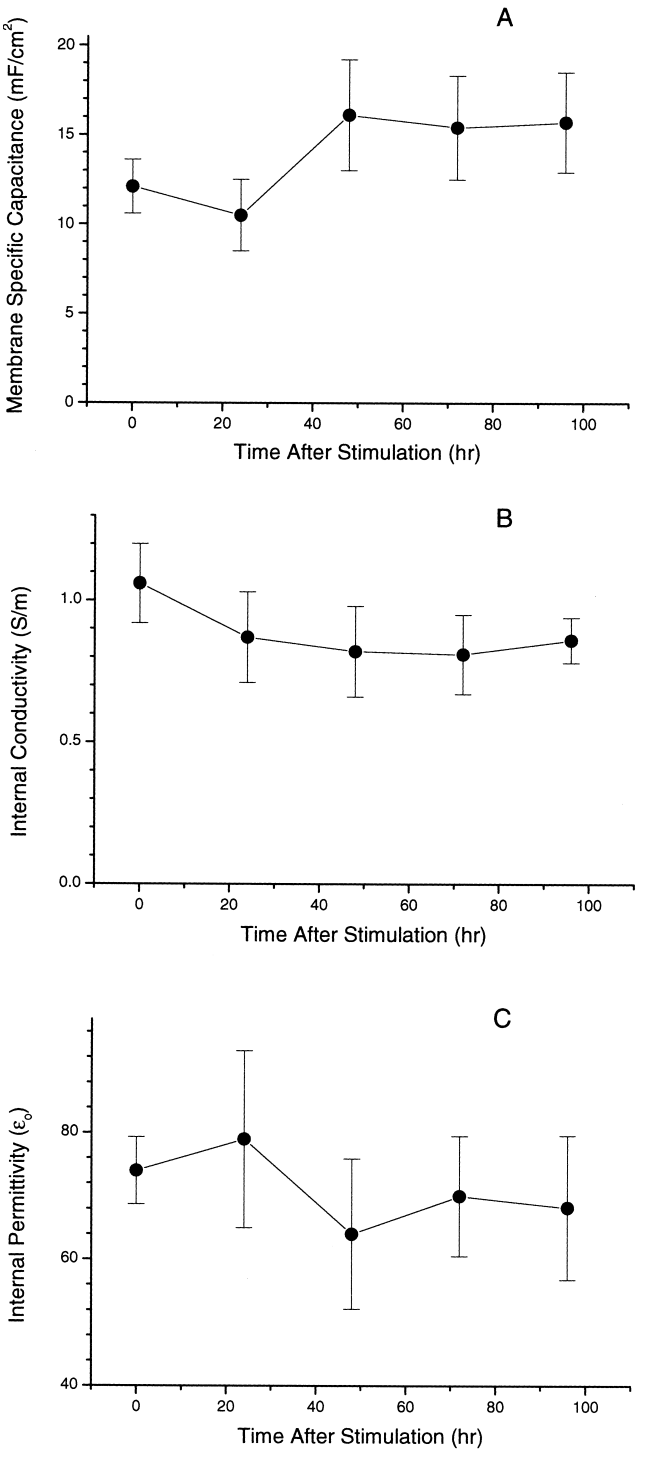


Table 1
Cell cycle distribution for T-lymphocytes as a function of the time after mitogenic stimulation

| Time (h) | $G_0/G_1$ | S | $G_2/M$ |
|---|---|---|---|
| 0 | 95.2 ± 0.9 | 2.6 ± 2.7 | 2.2 ± 1.8 |
| 24 | 89.5 ± 0.2 | 5.5 ± 3.2 | 5.0 ± 2.8 |
| 48 | 66.1 ± 5.1 | 17.3 ± 2.3 | 16.6 ± 4.8 |
| 72 | 65.3 ± 2.5 | 17.4 ± 0.7 | 17.3 ± 1.8 |
| 96 | 63.4 ± 7.3 | 18.7 ± 4.2 | 18.0 ± 2.2 |

The results are the mean and standard deviation of three separate sets of experiments.

### 3.4. Dielectric parameters for T-lymphocytes

An optimization algorithm was applied to determine the cell dielectric parameters from measured ROT spectra. Despite the fact that cells contained a membrane-enclosed nucleus, for which a three-shell model [4] would be more appropriate, a single-shell model was used for the analysis of ROT spectra. This choice was made because the effect of the cell nucleus are relatively small on the ROT spectra under our experimental condition, as evidenced by small differences observed between the ROT spectra of single-shell and three-shell particles when the inner sphere volume is less than 50% of the total volume [8]. Furthermore, as shown earlier, the measured

←

Fig. 4. Time dependency of membrane specific capacitance, internal conductivity and permittivity for human T-lymphocytes after mitogenic stimulation. Error bars indicate the standard deviations for all the cells from each sample. It is important to note that, for the cells studied at 24–96 h after stimulation by ROT, a deliberate choice was made to measure the large cells in the heterogeneous population so that we could measure cells that had responded to mitogenic stimulation and were in the S and $G_2/M$ phases of the division cycle.

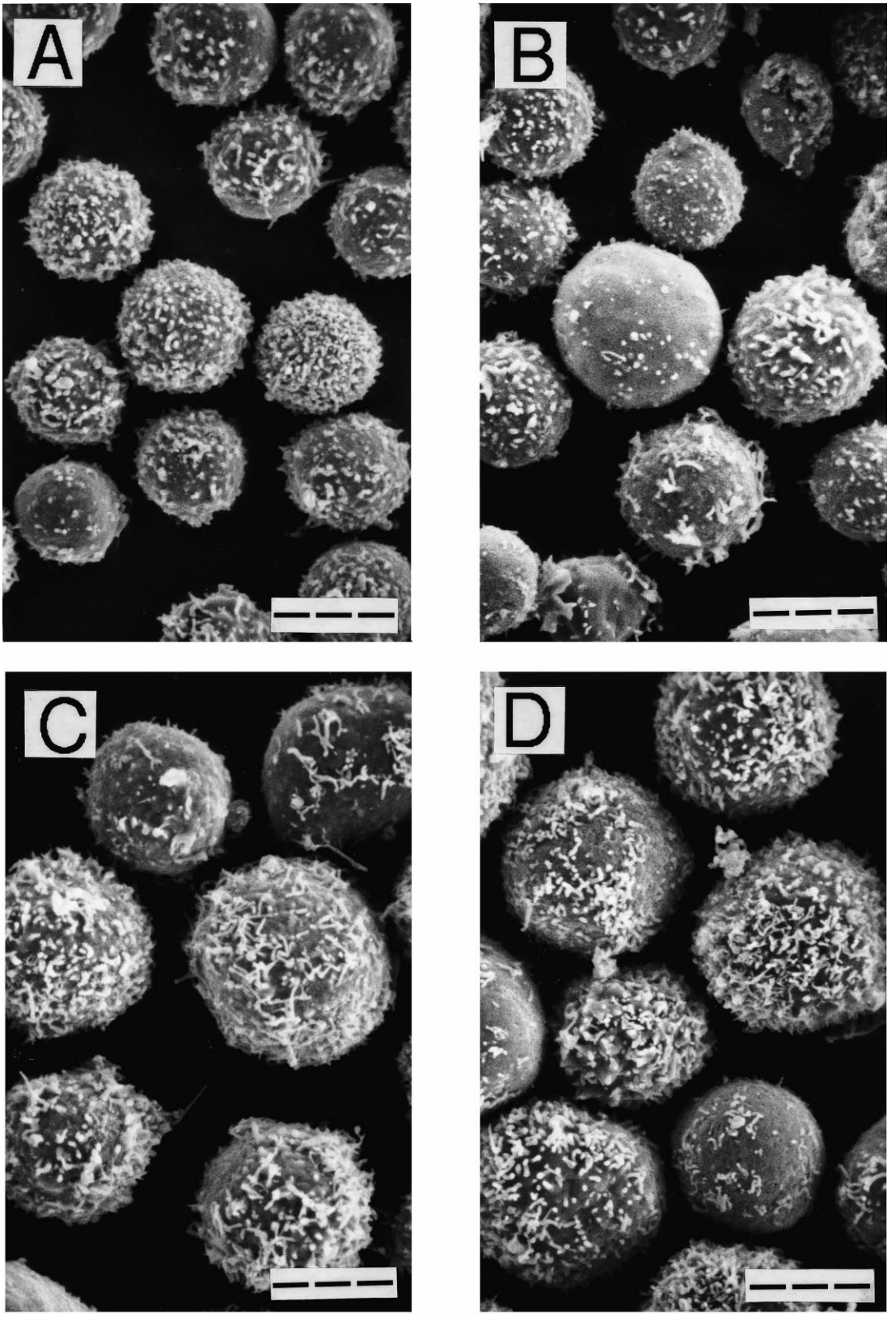


Fig. 5. Scanning electron micrographs of human T-lymphocytes at: (A) 0, (B) 24, (C) 48, and (D) 72 h after mitogenic stimulation. Bar length: 6 μm.

Table 2
Specific membrane capacitance, total capacitance, internal conductivity, and permittivity for human T-lymphocytes as a function of the time after mitogenic stimulation.

| Time (h) | $n$ | Radius (μm) | $C_{mem}$ (mF/m$^2$) | $C_{total}$ (pF) | $\sigma_{int}$ (S/m) | $\varepsilon_{int}$ |
|---|---|---|---|---|---|---|
| 0 | 6 | 3.03 ± 0.15 | 12.1 ± 1.5 | 1.40 ± 0.31 | 1.06 ± 0.14 | 74.0 ± 5.3 |
| 24 | 11 | 3.65 ± 0.33 | 10.5 ± 02.0 | 2.04 ± 0.59 | 0.87 ± 0.16 | 79.0 ± 14.0 |
| 48 | 14 | 4.54 ± 0.63 | 16.1 ± 3.1 | 4.03 ± 0.97 | 0.82 ± 0.16 | 64.0 ± 11.8 |
| 72 | 12 | 4.75 ± 0.56 | 15.4 ± 2.9 | 3.99 ± 1.34 | 0.81 ± 0.14 | 70.0 ± 9.5 |
| 96 | 12 | 4.69 ± 0.65 | 15.7 ± 2.8 | 4.45 ± 1.19 | 0.86 ± 0.08 | 68.2 ± 11.4 |
| 0 | 8 | 3.04 ± 0.26 | 12.1 ± 1.4 | 1.32 ± 0.32 | 1.11 ± 0.14 | 71.8 ± 9.7 |
| 24 | 8 | 3.92 ± 0.30 | 9.8 ± 1.6 | 1.70 ± 0.36 | 0.85 ± 0.15 | 74.5 ± 7.0 |
| 48 | 11 | 4.94 ± 0.63 | 1.54 ± 3.5 | 4.02 ± 1.18 | 0.84 ± 0.19 | 75.7 ± 13.3 |
| 72 | 8 | 5.40 ± 0.54 | 14.9 ± 2.9 | 4.78 ± 1.28 | 0.83 ± 0.11 | 72.4 ± 12.1 |
| 96 | 8 | 5.50 ± 0.67 | 16.2 ± 2.0 | 6.79 ± 1.14 | 0.83 ± 0.11 | 73.2 ± 9.2 |
| 0 | 8 | 3.04 ± 0.39 | 11.7 ± 1.6 | 1.42 ± 0.42 | 1.14 ± 0.17 | 66.0 ± 14.2 |
| 24 | 11 | 3.77 ± 0.41 | 9.6 ± 0.7 | 1.49 ± 0.22 | 0.79 ± 0.13 | 78.0 ± 7.0 |
| 48 | 8 | 4.85 ± 0.82 | 16.7 ± 4.1 | 4.59 ± 0.88 | 0.77 ± 0.23 | 69.1 ± 13.6 |
| 72 | 10 | 5.39 ± 0.62 | 16.5 ± 2.1 | 6.10 ± 1.50 | 0.77 ± 0.2 | 74.0 ± 13 |
| 96 | 10 | 5.11 ± 0.63 | 15.3 ± 2.6 | 5.05 ± 1.03 | 0.88 ± 0.14 | 72.0 ± 13.2 |

Results are means and standard deviations for $n$ cells from each sample.

ROT spectra alone are not sufficient to provide accurate estimates of the dielectric parameters of a three-shell model [8,25].

The dielectric parameters derived from ROT measurements are summarized in Table 2 for three sets of T-lymphocyte stimulation experiments. Since the results were similar for the three sets of experiments, only the derived data for the first set is shown in Fig. 4 in the form of time dependency of membrane capacitance, internal conductivity and permittivity after cell stimulation. The average specific capacitance decreased from 12 to 10 mF/m$^2$ ($\sim$15%) during the first 24 h following stimulation. Between 24 and 48 h, the capacitance value increased sharply from 10 to 16 mF/m$^2$ ($\sim$60%), and remained relatively constant thereafter. The average internal conductivity decreased from $\sim$1.1 to 0.8 S/m at 24 h after stimulation and remained at that value thereafter. The average internal permittivity (65–78) remained more or less unchanged throughout the course of the activation.

### 3.5. SEM studies

Fig. 5 shows representative scanning electron micrographs of T-lymphocytes prior to stimulation and at 24, 48, and 72 h after stimulation. Several findings are evident in these pictures. Prior to stimulation, T-lymphocytes appeared to be homogeneous in both size ($\sim$6 μm in diameter) and surface morphology. Cells exhibited some short ($<$0.2 μm) microvilli with a surface density less than 2 microvilli/μm$^2$. At 24 h after stimulation, some cells increased in size (to $\sim$7 μm in diameter) but with no significant difference in their surface morphology. At 48 h after stimulation, however, SEM revealed that large changes occurred in both cell size and surface morphology. There was a large range in size distribution, with cells showing diameters from 7 to 11 μm. Some cells (typically larger ones) exhibited extensive microvilli (up to 3 μm in length and 5 microvilli/μm$^2$ in density); others displayed morphology consistent with that seen prior to stimulation. Such a heterogeneous distribution of size and surface characteristics also was observed for the cells at 72 and 96 h after stimulation.

## 4. Discussion

### 4.1. Membrane capacitance

The membrane specific capacitance $C_{mem}$ found here for unstimulated human T-lymphocytes

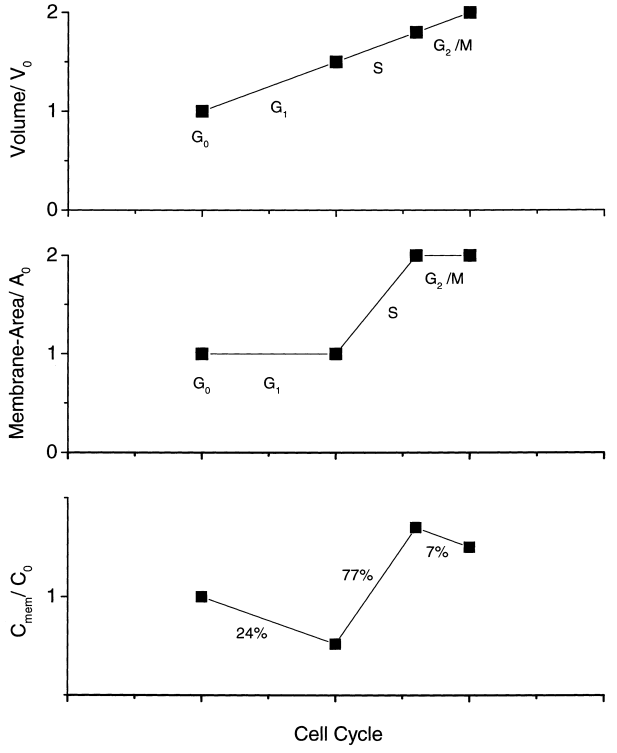


Fig. 6. Dependency of membrane specific capacitance on the cell cycle. $C_0$, $A_0$ and $V_0$ refer to the membrane specific capacitance, the membrane area and the cell volume at the start-point of $G_1$ phase, respectively. The analysis is based the assumption that the cell continuously increases its volume throughout the cycle, and the doubling of the membrane area only takes place in the S phase. The duration for $G_1$, S, and $G_2$/M phases is assumed to be 50, 30 and 20%, respectively, of the total cycle period. It is worthwhile to note that the change in membrane specific capacitance does depend on the relative duration of the $G_1$, S and $G_2$/M phases.

(12 mF/m$^2$) is in an excellent agreement with the value (12.1 ± 1.4 mF/m$^2$) reported by Arnold and co-workers using ROT on T-lymphocytes that had been separated electrophoretically from human blood (Arnold's results were briefly described in [3]). These $C_{mem}$ values for human T-lymphocytes are somewhat larger than those for various animal leukocytes reported elsewhere in the literature [3,20,26]. For example, values of 7.6, 8.6, and 9.1 mF/m$^2$ were reported for mouse T-lymphocytes [3], mouse splenocytes [20], and mixed rabbit leukocytes [26], respectively. These differences in membrane specific capacitances suggest that there are structural and compositional differences between the lymphocytes of different species.

In agreement with the earlier finding [3] that $C_{mem}$ increased for mouse lymphocytes after mitogenic stimulation, we observed that $C_{mem}$ for human T-lymphocytes increased from 12 mF/m$^2$ at $G_0$ to 16 mF/m$^2$ at 48 h after stimulation. It is important to note that $C_{mem}$ is a parameter that reflects a surface property per unit area [2,3,6,7,10], and the increase in $C_{mem}$ after stimulation is not the result of the change in cell size. In fact, the increase in size as cells entered the cell division cycle after stimulation would have caused a reduction in $C_{mem}$ if the total membrane capacitance were conserved.

We and others [2,3,6,7,10] have analyzed the physical factors that can affect the specific membrane capacitance and have concluded that an important factor determining $C_{mem}$ is the membrane surface configuration. Membrane features such as microvilli, ruffles, folds, and blebs increase the total membrane capacitance ($C_{total} = \varepsilon_{mem} A/d$, $\varepsilon_{mem}$ is the average dielectric permittivity of membrane, $A$ and $d$ are membrane area and thickness, respectively) and the specific $C_{mem}$ value ($C_{mem} = C_{total}/(\pi\ D^2)$, $D$ is the average cell diameter). As evidenced from the SEM studies (Fig. 5), T-lymphocytes after stimulation displayed increased surface complexity in terms of microvilli size and density. We believe that these changes in surface morphology are the main cause for the increase in membrane specific capacitance [6,7,10].

It also is interesting to note that the average cell total capacitance, reflecting the overall membrane surface area, increased from ~1.4 pF to as high as 6.8 pF. Thus, the total membrane area for a T-lymphocyte increased more than four times after stimulation as a result of both increased size and surface complexity.

### 4.2. Internal conductivity

As shown in Table 2, cell internal conductivity dropped from 1.1 to ~0.8 S/m at 24 h after stimulation, consistent with a qualitative assessment described in previously [18], which showed that the stimulated lymphocytes possess lower internal conductivity than unstimulated cells. This change coincided with a reduction in the membrane specific capacitance (from 12 to 10 mF/m$^2$) and preceded the large increase in $C_{mem}$ that occurred 24–48 h after

stimulation. This timing suggests that during entry to the cell division cycle, significant biological events occur within the T-lymphocyte interior prior to the net accumulation of the cell membrane. During the first 24 h following the stimulation, some cells left the $G_0$ phase to enter $G_1$ phase. These cells increased their volume and cytoplasmic space [27]. As a result, the volume ratio of the nucleus to the whole cell decreased. These changes occurred in $G_1$ phase, ahead of the S phase-dependent net accumulation of phospholipid in the membrane [28,29]. ROT spectra of cells exhibiting such changes in their cell interior were simulated using a three-shell model and were then fitted with a single-shell model. It was observed that, depending on the dielectric parameters used in the simulation, the derived internal conductivity using a single-shell model for the cells with a larger nucleus to cell volume ratio was 5–10% bigger than that for the cells having a smaller ratio. Therefore, the change in volume fraction of the nucleus in the cells after stimulation was probably at least partially responsible for the apparent change in internal conductivity.

### 4.3. Plasma membrane changes during the cell division cycle

First, we will present a general consideration of the dependency of membrane specific capacitance on the phase of the cell division cycle for a cell. A basic assumption for this analysis is that to double its volume, the cell continuously grows throughout the cell division cycle. It is now generally accepted that during $G_1$ phase there is a rapid synthesis and degradation of phospholipids [28,29]. Phospholipid metabolism is so rapid that some cells may turn over 75% of the total lipids during $G_1$ phase. However, there is no net accumulation of phospholipids [28,29]. If we take non-accumulation of membrane lipids as an indication that there is no net increase in the overall plasma membrane, then the increase in cell size would lead to a smoothing of the membrane features and, therefore, a resultant decrease in the membrane specific capacitance. If we assume that $G_1$ occupies 50% of the division cycle, then $C_{mem}$ would drop by 24% at the $G_1$/S phase boundary as a result of increases in cell volume and corresponding smoothing of the existing plasma membrane.

It also has been established that there is coordination between S phase DNA synthesis and net membrane phospholipid accumulation [28,29]. During S phase, membrane lipid turnover ceases, and the cells double their membrane phospholipid content in preparation for cell division. If we take this increase in phospholipids as an indicator for the increase in cell membrane area, then the total membrane capacitance should increase two-fold by the end of S phase. If we assume that S phase occupies 30% of the cell division cycle, taking into account the increase in cell size, the specific membrane capacitance $C_{mem}$ should then increase by 77% during S phase.

As cells enter the $G_2$/M phases, there is a cessation of phospholipid metabolism where both synthesis and degradation of membrane lipid components reach their minim [28,29]. Therefore, we can assume that there is no net increase in plasma membrane area in $G_2$/M phases. However, because cells continue to grow in $G_2$/M prior to the division, $C_{mem}$ should fall from its value at the S/$G_2$ boundary. If the $G_2$/M phase occupies 20% of the cell division cycle, then the membrane capacitance $C_{mem}$ should decrease by approximately 7% due to cell volume increases during the $G_2$/M phase. A schematic representation of the dependency of the membrane specific capacitance based on the above assumptions is shown in Fig. 6.

### 4.4. Relationship between cell cycle and cell dielectric parameters

The initial 24 h after stimulation was characterized by many T-lymphocytes leaving the $G_0$ to enter the $G_1$ phase. As determined from the FACS analyzer, 90% of cells were in $G_0$/$G_1$ phase at this time. The average capacitance of these cells was $\sim$15% less than that of the cells prior to stimulation, as expected from the above discussion that cells going through the $G_1$ phase will exhibit an decrease in $C_{mem}$. Between 24 and 48 h after stimulation, the percentage of cells in the S and $G_2$/M phases increased significantly from $\sim$11 to $\sim$34%. Because the ROT measurements were made on the larger size cells, we can assume that most of them were in the S and $G_2$/M phases and thus these cells would be expected to have higher $C_{mem}$ values, accounting for the observed large specific capacitance values. The

above interpretation also applies to the large $C_{mem}$ values for the cells at 72 and 96 h after stimulation.

At 48–96 h after stimulation, cells exhibiting larger capacitance values tended to have smaller internal conductivities, suggesting an inherent relationship between the derived dielectric parameters. Such an inherent relationship may reflect that both the membrane capacitance and the internal conductivity are dependent on the phases of the cell division cycle.

These findings are significant from a practical point of view because dielectric differences between cells in different phases of the cell division cycle could be exploited for selective cell manipulation by dielectrophoresis. For example, by choosing the suspension conductivity and the frequency of the applied electric field, cells at the S and $G_2$/M phases, having larger size and membrane specific capacitance, can be made to exhibit positive dielectrophoresis, whereas those at the $G_1$ phase can be made to exhibit negative dielectrophoresis. This offers the possibility to separate the cells in the $G_1$ phase from those in the S and $G_2$/M phase using a dielectrophoretic retention method [14,15]. Alternatively, cells in different phases of the division cycle may be made to experience differential negative dielectrophoretic forces, therefore may be separated with dielectrophoretic-field-flow-fractionation technique [30,31]. Research is currently being conducted to separate the cells according to the cell cycle distribution using dielectrophoresis.

## Acknowledgements

We are grateful to Jamileh Noshari for help in the preparation of T-lymphocytes from buffy coat. We also thank Drs. G. De Gasperis, K. Koo, J. Vykoukal, X.-J. Wang, and J. Yang for helpful discussions and Dr. R. Ford for use of his FACS analyzer. SEM was conducted at the M.D. Anderson Cancer Center core SEM facility supported by NIH Core Grant P30-CA16672. We thank K. Dunner Jr. and Dr. C. Bucana for SEM sample preparation and imaging. This work was supported in part by National Institutes of Health Grant R01 DK51065-01 from the National Institute of Diabetes and Digestive and Kidney Disease and a Biomedical Engineering grant from the Whitaker Foundation.

## References

[1] W.M. Arnold, U. Zimmermann, J. Electrostat. 21 (1988) 151–191.
[2] W.M. Arnold, R.K. Schmutzler, S. Al-Hasani, D. Kerbs, U. Zimmermann, Biochim. Biophys. Acta 979 (1989) 142–146.
[3] X. Hu, W.M. Arnold, U. Zimmermann, Biochim. Biophys. Acta 1021 (1990) 191–200.
[4] Y. Huang, R. Hölzel, R. Pethig, X.-B. Wang, Phys. Med. Biol. 37 (1992) 1499–1517.
[5] R. Hölzel, I. Lamprecht, Biochim. Biophys. Acta 1104 (1992) 195–200.
[6] V.L. Sukhorukov, C.S. Djuzenova, W.M. Arnold, U. Zimmermann, J. Membr. Biol. 142 (1994) 77–92.
[7] X.-B. Wang, Y. Huang, P.R.C. Gascoyne, F.F. Becker, R. Hölzel, R. Pethig, Biochim. Biophys. Acta 1193 (1994) 330–344.
[8] Y. Huang, X.-B. Wang, R. Hölzel, F.F. Becker, P.R.C. Gascoyne, Phys. Med. Biol. 40 (1995) 1789–1806.
[9] G. Fuhr, R. Hagedorn, in: P.T. Lynch, M.R. Davey (Eds.), Electrical Manipulation of Cells, 1996, Charmian & Hall, New York, pp. 37–70.
[10] Y. Huang, X.-B. Wang, F.F. Becker, P.R.C. Gascoyne, Biochim. Biophys. Acta 1282 (1996) 76–84.
[11] J. Gimsa, T. Muller, T. Schnelle, G. Fuhr, Biophys. J. 71 (1996) 495–506.
[12] M. Kurschner, K. Nielsen, C. Andersen, V.L. Sukhorukov, W.A. Schenk, R. Benz, U. Zimmermann, Biophys. J. 74 (1998) 3031–3043.
[13] V.L. Sukhorukov, U. Zimmermann, J. Membr. Biol. 153 (1996) 161–169.
[14] F.F. Becker, X.-B. Wang, Y. Huang, R. Pethig, J. Vykoukal, P.R.C. Gascoyne, J. Phys. D: Appl. Phys. 27 (1994) 2659–2662.
[15] F.F. Becker, X.-B. Wang, Y. Huang, R. Pethig, J. Vykoukal, P.R.C. Gascoyne, Proc. Natl. Acad. Sci. USA 92 (1995) 860–864.
[16] Y. Huang, X.-B. Wang, F.F. Becker, P.R.C. Gascoyne, Biophys. J. 73 (1997) 1118–1129.
[17] G. Fuhr, U. Zimmermann, S.G. Shirley, in: U. Zimmermann, G.A. Neil (Eds.), Electromanipulation of Cells, 1995, CRC Press, Boca Raton, pp. 259–328.
[18] H. Ziervogel, R. Glaser, D. Schadow, S. Heymann, Biosci. Rep. 6 (1986) 973–980.
[19] A. Surowiec, S.S. Stuchly, C. Izaguirre, Phys. Med. Biol. 31 (1986) 43–53.
[20] K. Asami, Y. Takahashi, S. Takashima, Biochim. Biophys. Acta 1010 (1989) 49–56.
[21] A. Boyum, Scand. J. Clin. Lab. Invest. 21, (Suppl. 97) (1968) 77–89.
[22] K.L. Donaldson, A. Mcshea, A.F. Wahl, J. Immunol. Methods 203 (1997) 25–33.
[23] K.L. Donaldson, A. Mcshea, A.F. Wahl, J. Immunol. Methods 203 (1997) 25–33.
[24] Y. Huang, R. Pethig, Meas. Sci. Technol. 2 (1991) 1142–1146.

[25] P.R.C. Gascoyne, F.F. Becker, X.-B. Wang, Bioelectron. Bioenerget. 36 (1995) 115–125.
[26] H. Fricke, Nature 172 (1953) 731–734.
[27] A.L. Maizel, S.R. Mahta, S. Hauft, D. Franzini, L.B. Lacaman, R.J. Ford, J. Immunol. 127 (1981) 1058–1064.
[28] S. Jackowski, J. Biol. Chem. 271 (1996) 20219–20222.
[29] S. Jackowshi, J. Biol. Chem. 269 (1994) 3858–3867.
[30] Y. Huang, X.-B. Wang, F.F. Becker, P.R.C. Gascoyne, Biophys. J. 73 (1997) 1118–1129.
[31] X.-B. Wang, J. Vykoukal, F.F. Becker, P.R.C. Gascoyne, Biophys. J. 73 (1998) 2689–2701.